

# MAPPING OF CHLOROPHYLL AND SUSPENDED PARTICULATE MATTER MAPS FROM CHRIS IMAGERY OF THE OOSTENDE CORE SITE

Barbara Van Mol, Young-Je Park, Kevin Ruddick, Bouchra Nechad

Management Unit of the North Sea Mathematical Models (MUMM), Royal Belgian Institute for Natural Sciences (RBINS), 100 Gulledele, B-1200 Brussels, Belgium. Email : B.VanMol@mumm.ac.be

## 1. ABSTRACT

The image set created on 5 August 2003 by CHRIS/PROBA is analyzed to assess the feasibility of producing suspended particulate matter (SPM) and chlorophyll (CHL) maps. To produce these maps images are first destriped, atmospherically corrected and georeferenced. Once the data processing is finished, the results are compared with seaborne measurements and data products retrieved from other ocean colour sensors. The data processing with its associated problems, the comparison with seaborne and other data and the creation of SPM and CHL maps are described in this paper. Conclusions and recommendations are made in the context of considering CHRIS/PROBA as a model for the future generation of small ocean colour missions.

## 2. INTRODUCTION

Mapping of chlorophyll-a (CHL) concentration is required to assess the eutrophication of the Belgian waters [1, 2]. Further interest comes from marine scientists, for whom CHL maps would provide information on the marine ecosystem, and especially for ecosystem modelers who require data for model validation [2]. The interest in maps for Suspended Particulate Matter (SPM) concentrations in Belgian coastal waters is associated with the need to provide boundary, initial and validation data for sediment transport models [3].

While seaborne measurements of CHL and SPM provide high quality (low uncertainty) data for a limited number of locations, mapping of a large area is confounded by very sparse spatial coverage and, for highly dynamic tidal waters, by the asynchronicity of measurements. Satellite mapping offers the potential for covering large areas (+/- 13\*13 km<sup>2</sup> in the case of CHRIS) at a "snapshot" moment with resolution of spatial variability down to tens of meters, thus revealing features associated with fine-scale bathymetry and river discharges.

The potential for mapping of SPM and CHL has already been demonstrated for SeaWiFS and MERIS and is under development for MODIS. CHRIS/PROBA must be considered as a relatively low budget technology-proving mission in comparison to these

well-supported operational or pre-operational ocean

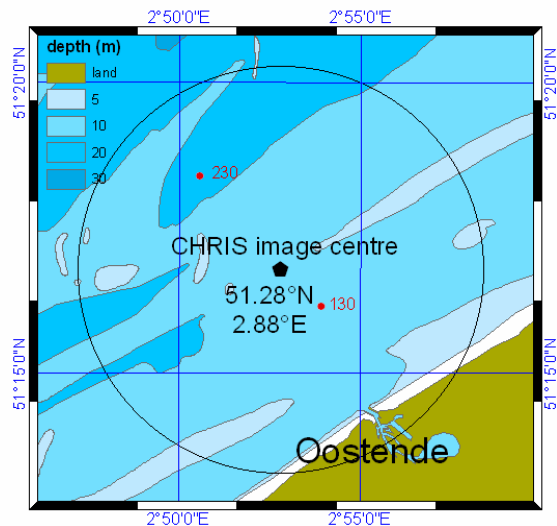


Fig. 1: Oostende Core site

colour sensors, which provide daily global coverage for a large user base. However, the interest in CHRIS/PROBA lies in a number of original technological features which may form the basis of a future generation of ocean colour sensors:

- Economic constraints are likely to lead over the next twenty years to preference for small satellites with a very limited number of sensors (e.g. one) facilitating system design and launch. In this sense PROBA is seen as a model for a new generation of small low-cost satellites with consequent challenges for system engineers and for product developers.
- The optical complexity of coastal and inland waters and their overlying atmosphere drives a need for much greater spectral resolution than is available on current ocean colour sensors, e.g. to separate phytoplankton absorption from coloured dissolved organic matter (CDOM) absorption or to perform accurate atmospheric correction for turbid waters. It is becoming clear that the future for coastal and inland waters is hyperspectral and CHRIS thus offers a first chance to test future algorithms.
- Pointability of the platform allows imaging of the same sea area from different angles, thus offering more information for use in correction of atmospheric and air-sea interface effects, as used by AATSR for sea surface temperature measurements. In a more general context pointable platforms offer

the possibility of on-demand imaging for example in the case of special events, as used already for terrestrial applications in SPOT series.

- Finally, the high spatial resolution of CHRIS is more comparable to that of terrestrial sensors such as Landsat and SPOT than to that of ocean colour sensors (e.g. 1.1 km for SeaWiFS, 250m for MERIS) and offers the possibility of mapping much smaller features for example in nearshore, estuarine or inland waters.

These potential advantages of the CHRIS/PROBA system are discussed here in the framework of production of CHL and SPM maps for coastal waters as tested specifically for the Oostende core site (Fig. 1). CHRIS mode one produces imagery with a spatial resolution of 30\*30m<sup>2</sup> and 62 spectral bands which cover wavelengths from 411 nm up to 997 nm.

The final objective is to assess the potential of multi-look angle hyperspectral imagery for SPM and CHL mapping. To reach this objective the raw CHRIS/PROBA images are processed and the detectability of SPM and CHL is investigated. This paper describes the image processing steps, describes problems encountered and gives preliminary SPM and CHL maps.

Since the launch of CHRIS/PROBA, 10 datasets of the core site Oostende have been acquired (Table 1). In this paper only the dataset acquired on 5 August 2003 is considered in detail because this day was cloud free and simultaneous seaborne measurements are available.

Table 1: data acquisition at the Oostende core site

Date	n° images	CHRIS data	Sea data
21/06/2002	5	clouded	4 stations
26/07/2002	5	clouded	2 stations
05/03/2003	5	clouded	No
19/06/2003	5	clouded	3 stations
27/06/2003	4	clouded	3 stations
21/07/2003	3	partially clouded	No
05/08/2003	5	clear	2 stations
06/08/2003	5	partially clouded	3 stations
20/09/2003	5	clear	No
21/09/2003	3	clear	No

### 3. METHOD

The image processing can be subdivided into four steps: destriping, atmospheric correction, georeferencing and SPM/CHL retrieval. All the image processing is done with ENVI/IDL software version 4.0. CHRIS/PROBA data for water-leaving reflectance, SPM and CHL is then compared with seaborne data and with other sensors.

#### 3.1 Destriping

All the retrieved data show “vertical lines” on the image (Fig.2). Each image has these vertical lines at the same pixels, suggesting a sensor problem. To minimize this problem a correction factor for each column is calculated, individually for each band and image.

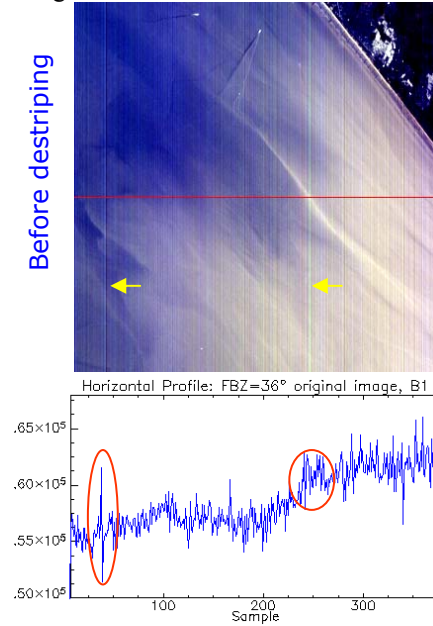


Fig. 2: unprocessed CHRIS/PROBA image. 5 August 2003, FBZ = 36°, 411nm, top of atmosphere radiance

The correction factors are based on a 5 column moving average. For each column (denoted  $i$ ) and each band (denoted  $k$ ) the column-average radiance (denoted  $L_{i,k}$ ) is calculated for a block of water pixels (Fig.3). A correction factor (denoted  $C_{i,k}$ )

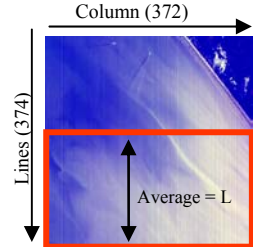


Fig.3: Block of water pixels used for calculation of column average radiance

is then calculated for each column by smoothing over 5 columns (Eq. 1):

$$C_{i,k} = \frac{L_{i-2,k} + L_{i-1,k} + L_{i,k} + L_{i+1,k} + L_{i+2,k}}{5 * L_{i,k}} \quad (1)$$

The variation of this correction factor over adjacent columns is about 1%.

#### 3.2 Atmospheric correction

The top-of-the atmosphere radiance measured by CHRIS is composed of the atmospheric path-, sea-surface- and water-leaving radiances. The quantity of

interest for marine applications is the water-leaving reflectance.

Two approaches were tried for subtracting the atmospheric path and sea-surface reflectance from the top-of-atmosphere reflectance: a simple method based on the darkest pixel and an alternative method based on a radiative transfer model.

### 3.2.1 Darkest pixel correction

This is a very simple correction, based on 2 assumptions:

- The first assumption is that in the darkest water pixel of the image there is total light absorption i.e. this pixel represents black water and the light recorded for this pixel is equal to the atmospheric path radiance.
- Secondly it is assumed that the atmospheric path radiance is uniform all over the image.

The spectrum of the darkest water pixel (assumed to represent the atmosphere) is subtracted from the whole image. The darkest pixel is found by searching for the lowest values over water for all wavelengths. The pixel with the lowest value in most of the bands was selected as the darkest pixel.

### 3.2.2 Radiative transfer model

The darkest pixel method described above is useful for achieving preliminary results and assessing sensor performance. However, a more accurate atmospheric correction requires use of a radiative transfer model to assess contributions to top-of-atmosphere reflectance from water-leaving reflectance (attenuated by transmission from sea to sensor) and from scattering of light by atmospheric particles (“aerosol” reflectance) and air molecules (“Rayleigh” reflectance). The algorithm of Gordon and Wang [4] with non-zero NIR water-leaving reflectance is used. Sun glint is neglected here because only the viewing angle away from sun is considered (image with Fly By Zenith angle, FBZ =  $-36^\circ$ ) and whitecaps are neglected because the sea was flat on 5 August 2003. Rayleigh reflectance was removed using the pre-computed look-up table for the zenith and azimuth angles of the sun and the sensor. However, aerosol reflectance cannot at present be calculated using the near infrared spectrum because of excessive noise there.

## 3.3 Georeferencing

Georeferencing the CHRIS/PROBA satellite images is a major problem for marine sites because no georeferencing information is supplied with imagery and ground control points (GCP) cannot be identified at sea. The test site was chosen to contain some land for GCP identification. The image of 5 August with the best recognizable land is chosen as base image. On this image 5 GCPs are identified. The image is

georeferenced by applying an image to map registration with 5 GCPs. After the registration, coordinates are inter- and extrapolated a rotation scaling translation transformation and nearest neighbour remapping.

This newly georeferenced image is used as the base map to georeference the other images from the 5 August set by an image to image registration.

## 3.4 Comparison with other data

### 3.4.1 Seaborne data



Fig.4: TriOS instruments

On 5 August 2003 seaborne measurements were made for two stations within the Oostende test site. The parameters measured are water-leaving reflectance, SPM and CHL. The water-leaving reflectance is measured by the TriOS instruments (fig. 4). This system comprises 3 sensors which are

mounted on the bow of the ship at zenith angles of  $0^\circ$ ,  $140^\circ$  and  $40^\circ$ , and measure respectively downwelling irreflectance, water leaving reflectance and sky reflectance following the protocol used by MUMM for MERIS validation [5] based on the NASA protocols [6]. Water samples are collected simultaneously with TriOS measurements and analyzed for SPM and CHL (using the HPLC method) in the MUMM laboratory at Oostende. The positions and times of the measurements are given in table 2.

### 3.4.2 Satellite reflectance data

On 5 August 2003 there were overpasses from MERIS and SeaWiFS. These satellites sensors produce images all over the world. The analyzed MERIS and SeaWiFS images have respectively a resolution of 1.1 km and 1.2 km and a spectral resolution of 15 bands from 412 to 900 nm and 8 bands from 412 to 865 nm.

Table 2: Radiometric data acquired on 5 August 2003

Sensor	UTC time	latitude	longitude	FBZ
TriOS/station 130	10:30	51.27	2.90	
TriOS/station 230	11:16	51.31	2.84	
CHRIS/image A	11:11:42	51.28	2.88	$36^\circ$
CHRIS/image 9	11:12:31	51.28	2.88	$0^\circ$
CHRIS/image B	11:13:20	51.28	2.88	$-36^\circ$
MERIS	10:25:31			
SEAWIFS	13:02:39			

The spectra from the different sensors are compared at station 130 and station 230. Only the images with FBZ 36°, 0° and -36° are taken into consideration as the georeferencing from the other images is not accurate enough and station 130 falls out of the image.

### 3.5 Creation of suspended particulate matter maps (SPM) and chlorophyll-a (CHL) maps

After the image processing Eq.2 is used to transform CHRIS images from reflectance into reflectance [7].

$$\rho_w = \frac{L_w * \pi}{E_d} \quad (2)$$

where  $\rho_w$  = water leaving reflectance,  $L_w$  = above water leaving reflectance and  $E_d$  = above water downwelling reflectance. The  $E_d$  used in the calculations comes from the TriOS measurements and is corrected for time difference. As the creation of SPM and CHL maps based on CHRIS/PROBA imagery is still in a test phase, the algorithms are only applied on image CHRIS\_OT\_030805\_367B\_31.hdf with FBZ= -36°. This image was taken on 5 August 2003 and is selected for processing because it has no sunglint, no drop-out lines and the two stations with seaborne measurements fall inside the image.

#### 3.5.1 Suspended Particulate Matter

The retrieval of SPM maps is based on the Eq. 3

$$SPM(g/m^3) = A_Q \frac{\rho_w}{0.187 - \rho_w} + B_Q \quad (3)$$

where  $A_Q$  and  $B_Q$  are wavelength dependent and calibrated using the method of [7]. For the production of SPM maps the wavelength 555 nm was chosen with  $A_Q = 25.99$  mg/l and  $B_Q = 4.98$  mg/l.

#### 3.5.1 Chlorophyll

For transforming the reflectance maps into chlorophyll maps the wavelengths 664nm, 708nm, and 778nm are used as in Eq. 4-6 [2] based on the work on [8].

$$b_{b0} = 1.2 * 2.69m^{-1} * \frac{\rho_{w,778nm}}{0.187 - \rho_{w,778nm}} \quad (4)$$

$$\gamma = \frac{\rho_{w,708nm}}{\rho_{w,664nm}} \quad (5)$$

$$CHL(mg/m^3) = \frac{1}{0.0146m^2mg^{-1}} * \left[ (\gamma * 0.699m^{-1} + b_{b0}) - 0.402m^{-1} - b_{b0} \right] \quad (6)$$

## 4. RESULTS AND DISCUSSION

### 4.1 Destriping

Applying the correction factors described in 3.1 results in a much smoother image than the original (Fig. 5). Outliers are greatly reduced but not eliminated completely.

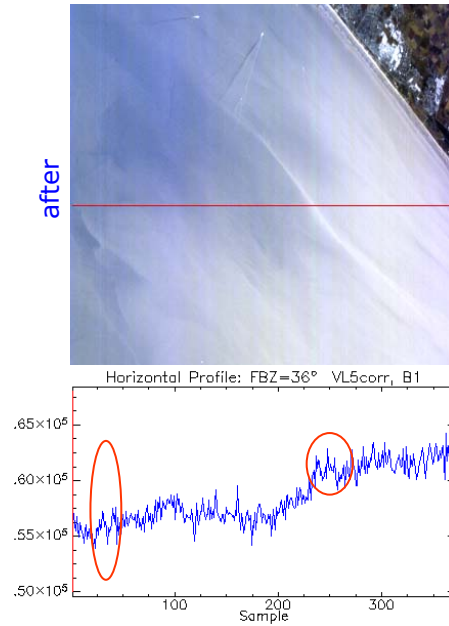


Fig. 5: destriped CHRIS/PROBA image. 5 August 2003, FBZ = 36°, 411nm

### 4.2 Atmospheric correction

#### 4.2.1 Darkest pixel correction

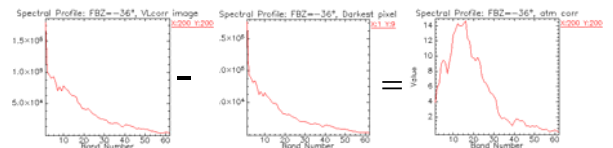


Fig.6: darkest pixel atmospheric correction

Subtracting the spectrum of the darkest pixel from the whole image results in spectra with a typical shape for water masses. The weakness of this correction lies in the two assumptions. Because the water even in the darkest pixel is not perfectly black, there is an overestimation of the atmospheric path reflectance. This results in an underestimation of the water leaving reflectance. The assumption of an equal atmosphere all over the image site has less consequence on a clear day

then on a clouded day. Despite such drawbacks the darkest pixel approach provides an acceptable data.

#### 4.2.2 Radiative transfer model

The radiative transfer model is a more accurate method to calculate the atmospheric correction than the darkest pixel approach if all factors can be calculated properly. Unfortunately this is not yet the case for the CHRIS/PROBA sensor which provides images with considerable spectral noise. Because of these variations it is impossible to estimate the spectral slope which is needed to calculate the aerosol reflectance, one of the input parameters for the model.

It could be possible to smooth the spectra and in this way estimate the spectral slope, but it is preferred not to do this at this stage because this would hide a sensor problem which could be solved more comprehensively for example by increasing electronic gain [9]. Another problem is the unrealistic values in the lowest band for wavelength 410 nm.

Therefore the darkest pixel atmospheric correction is preferred above the radiative transfer model until smoother spectral data becomes available.

#### 4.3 Georeferencing

Georeferencing images by the use of 5 ground control point (GCPs) on land gives a good result for the interpolated points on land but the error increases for extrapolated points far from the GCPs. This approach is not very accurate because all GCPs are located in the same corner of the image. The GCP location error for any image is typically half a pixel, if ground control points like for example a cross road, the corner of a bridge, a pool in a park are identified correctly. Here this uncertainty is amplified considerably going from the land corner of the image to the opposite sea corner. Georeferencing image to image assumes that the base image is perfectly georeferenced. Otherwise the georeference errors of the base image are extrapolated to the other images.

The results of georeferencing the images from 5 August 2003 are acceptable for the land and points close to land but information about georeferencing or even the nominal size, location and orientation of the image would lead to better results. Figure 7 shows the difference between the original image and the same image after destriping and georeferencing.

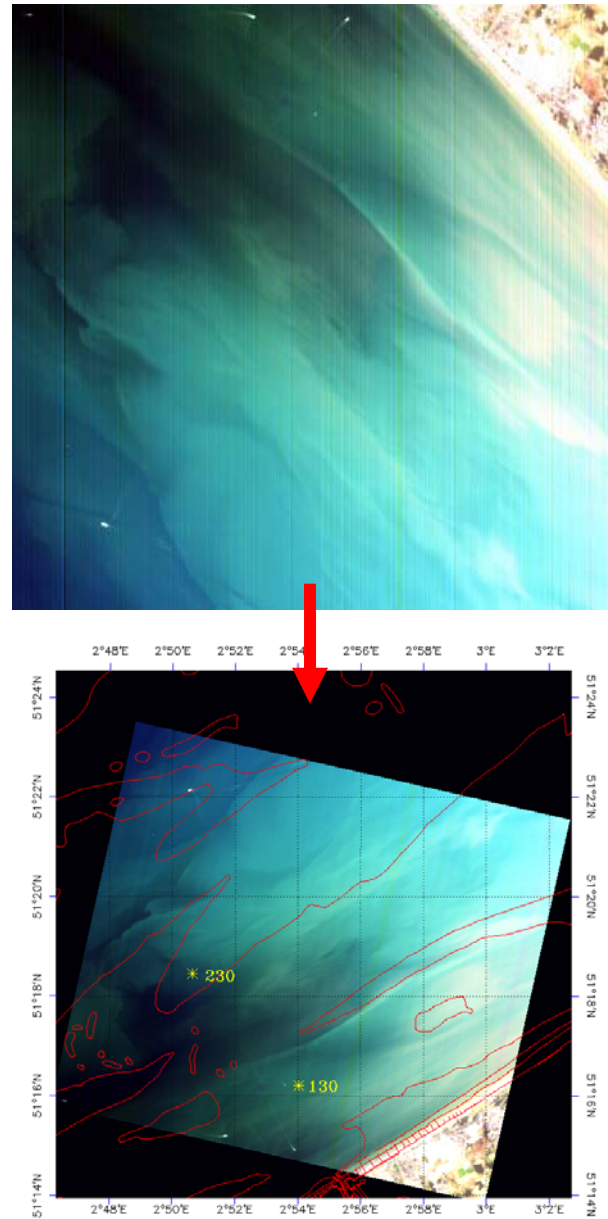


Figure 7: 5 August 2003, FBZ = -36°, RGB composite using 691nm, 561nm and 461nm before and after image processing.

#### 4.4 Comparison with other data

Figure 8 shows the water leaving reflectance spectra at station 130 and 230 for the CHRIS/PROBA images with FBZ -36°, 0° and 36° and for the TriOS measurements. Figure 9 presents the water reflectance spectra at station 130 and 230 for the CHRIS/PROBA images with FBZ -36°, 0° and 36°, TriOS, MERIS and SeaWiFS.

All sensors show a higher reflectance and reflectance at station 130. This is explained by the concentration of particles in suspension at station 130 which leads to a higher reflection. Analysis of the water samples for SPM shows the same tendency (table 3).

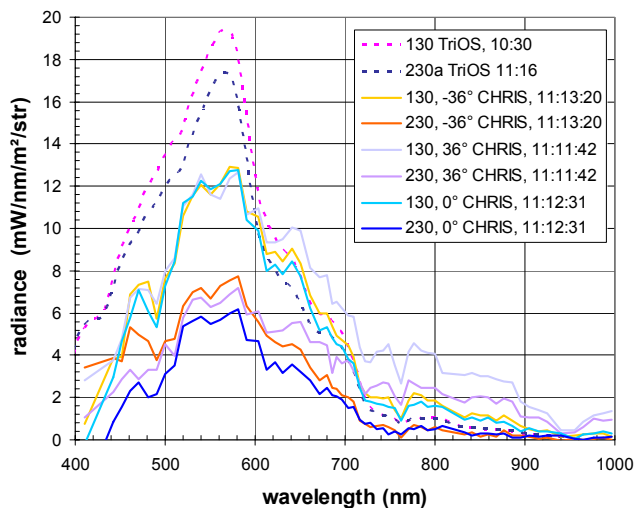


Fig.8: water-leaving radiance from seaborne and CHRIS satellite measurements of 5 August 2003

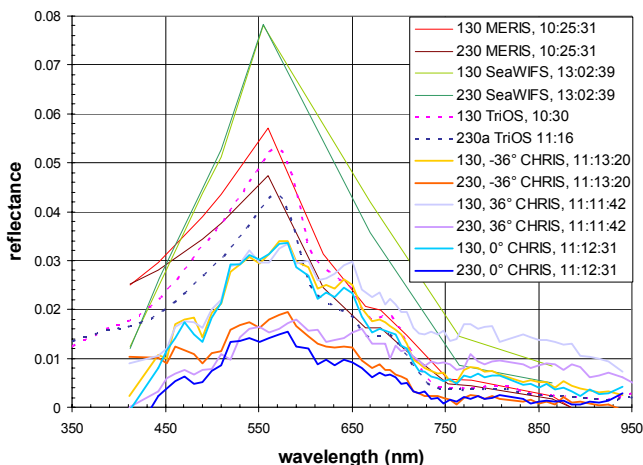


Fig.9: water-leaving reflectance from seaborne and satellite measurements of 5 August 2003

The values are lower for CHRIS/PROBA in comparison with other sensor data. This can be explained by the darkest water pixel assumption. Time differences may also affect the comparison.

The CHRIS/PROBA spectra are similar at station 130 for wavelengths until 600nm for the 3 look angles. Higher wavelengths show a discrepancy for the data from the CHRIS/PROBA image with FBZ equal to -36°, possibly due to sunglint. The CHRIS/PROBA spectra at station 230 show more variation between the different view angles. These variations could be due to the increased georeferencing error further from land.

The CHRIS/PROBA radiance and reflectance spectra show spectral noise. This noise could be reduced by applying a spectral smoothing but because less is known about which values are correct and which are not, it is preferred at present not to smooth the spectra

until good correction factors are available because important data could be lost.

Table 3: Data from water samples

Station	Sample date	SPM mg/l	CHL a mg/m <sup>3</sup>
130	5/08/2003	8.20	11.37
230	5/08/2003	7.27	11.49

## 4.5 SPM and CHL maps

### 4.5.1 SPM maps

Figure 10 and 11 show SPM maps deduced from the reflectance at wavelength 551 nm for CHRIS/PROBA images with fly by zenith angle -36° and 0° respectively. The image with fly zenith angle 36° is not processed because of sunglint. The black lines at the bottom of figure 10 are drop-out lines, generated during the data acquisition. Both maps give similar results. SPM varies from +/- 4 to 25 mg/l. The calculated values for SPM are in the same range as the measured values (Table 4) The higher concentrations of SPM in the East are explained by a high turbidity zone in the Belgian/Dutch coastal area. The processes responsible for the high turbidity zone formation are the currents and the import of SPM through the Strait of Dover. Also the erosion of clay and Holocene mud layers is partly responsible for the increase of SPM concentration here. However, the Strait of Dover remains the major source of SPM [3].

Table 4: satellite vs. seaborne measured SPM concentrations

Station	SPM (mg/l) FBZ = -36°	SPM (mg/l) FBZ = 0°	Measured SPM (mg/l)
130	11.41	11.35	8.20
230	7.98	7.16	7.27

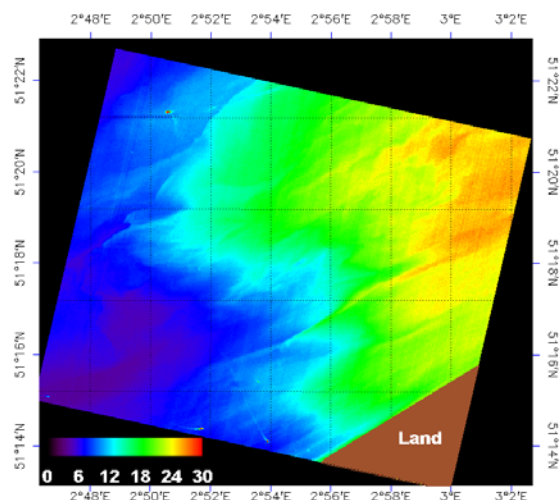


Figure 10: SPM map based on CHRIS/PROBA, 5 August 2003, FBZ = -36°, wavelength 551 nm

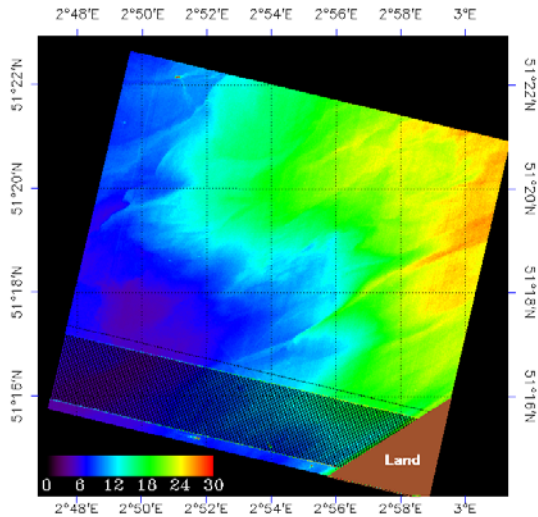


Figure 11: SPM map based on CHRIS/PROBA, 5 August 2003, FBZ = 0°, wavelength 551 nm

Comparison with the SPM maps deduced from MERIS (Fig. 12) and SeaWiFS (fig.13) shows agreement and indicate that the strong SPM gradient across the CHRIS image corresponds to a frontal region between high SPM waters near the coast between Oostende and the Scheldt and low SPM waters offshore and further West. The stability of this feature over the 2.5 hour period considered and its appearance in many other SeaWiFS and MERIS images confirm that CHRIS detects successfully SPM.

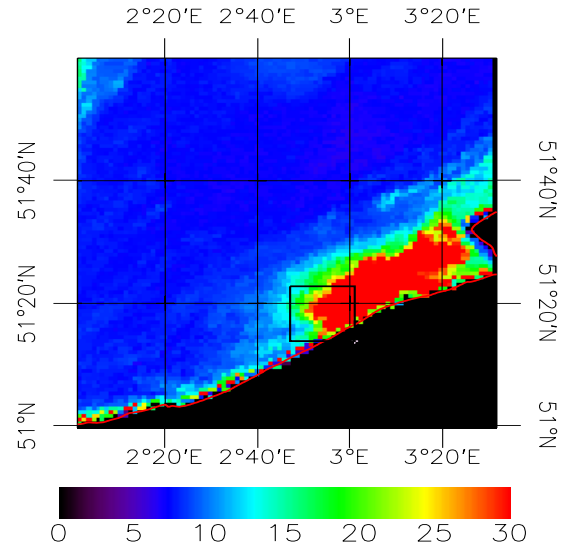


Fig. 13: SPM map deduced from SeaWiFS, 5 August 2003

#### 4.5.2 Chlorophyll maps

The chlorophyll map in figure 14 is deduced from the CHRIS/PROBA image with FBZ -36° and is based on 3 bands: 664 nm, 708 nm and 778 nm. At first sight it seems it might be possible to create chlorophyll maps from CHRIS/PROBA images since the CHL distribution in Fig.15 is not correlated with SPM nor with any obvious atmospheric feature. However, comparison with seaborne measurements and inspection of the highest values shows that the values are not realistic...yet (table 5).

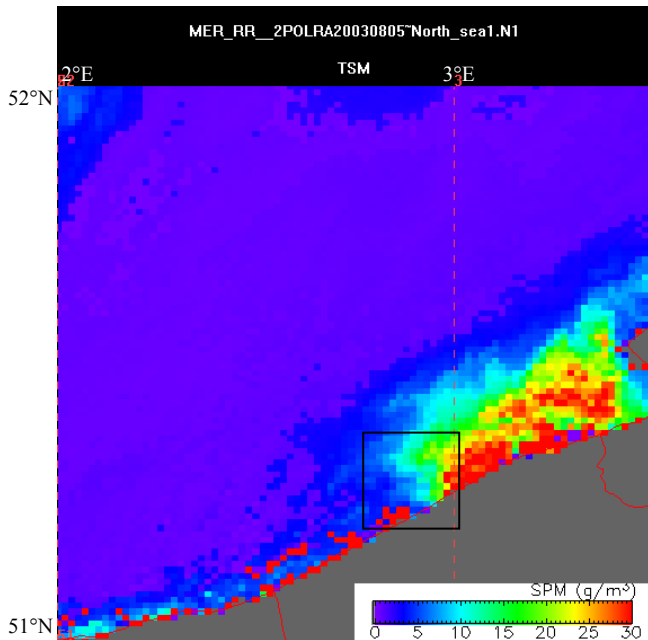


Fig. 12: SPM map deduced from MERIS, 5 August 2003

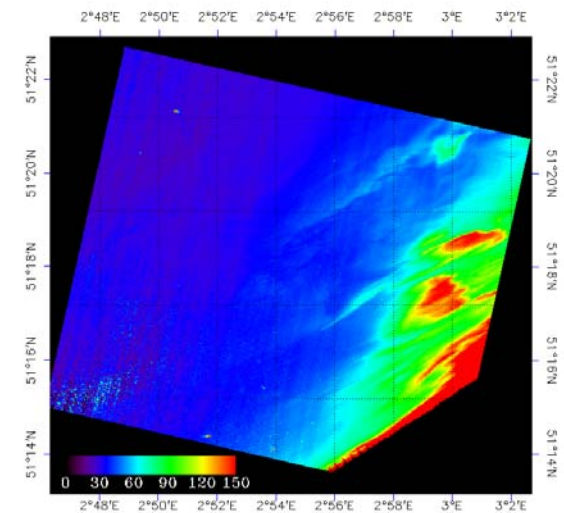


Fig. 14: chlorophyll map based on CHRIS/PROBA, 5 August 2003, FBZ = -36°

Table 5: Satellite vs. water sample CHL concentrations

Station	Satellite value (mg/m <sup>3</sup> )	Measured value (mg/m <sup>3</sup> )
130	39.27	11.37
230	32.25	11.49

## 5. CONCLUSION

The processing of CHRIS images involves some problems due to the data quality: vertical stripes, spectral noise, drop-out lines and strange values at band 1 (410 nm). Most of these problems are mitigated in the processing adopted here but a missionwide solution would be better. The major problem in the image processing of marine images is the georeferencing. As long as this problem is not solved properly, it is difficult to validate accurately the end products (SPM and chlorophyll maps) with seaborne measurements.

The simple dark pixel atmospheric correction gives reasonable results for the creation of SPM maps. An atmospheric correction by radiative transfer modeling would be better but requires better spectral data.

CHRIS/PROBA image data are good enough to create useful SPM maps. The possibility to create CHL maps needs further research.

The advantages of the different viewing angles are at this stage used only to eliminate sun glint. In the future the image set with different viewing angles may help to improve atmospheric correction or may be used as test data to validate sun glint algorithms e.g. for MERIS. The potential of multi-look angle hyperspectral imagery for suspended particulate matter and chlorophyll mapping remains promising but requires further assessment after improvement of image data and atmospheric correction.

## 6. ACKNOWLEDGEMENTS

This study was funded by the Belgian Science Policy Office in the framework of the BELCOLOUR project and by PRODEX contract 15189/01/NL/SFe(IC) The CHRIS/PROBA data was supplied by ESA/SIRA. The ESA/SIRA scientists and Peter Fletcher are thanked for their support. We thank Vera De Cauwer for the seaborne measurements and the Tuimelaar crew for their help. MUMM's Chemistry lab is thanked for the chlorophyll/SPM analysis.

## 7. REFERENCES

- [1] De Cauwer V., Ruddick K., Park Y., Nechad B. and Kyramarios M., 2004. *Optical remote sensing in support of eutrophication monitoring in the Southern North Sea*. EARSel eProceedings 3, 1/2004.
- [2] Ruddick K., Park Y. and Nechad B., 2003. *MERIS imagery of coastal waters: mapping of SPM and CHL*. European Space Agency, SP-549.
- [3] Fettweis M., Van den Eynde D., 2003. *The mud deposits and the high turbidity in the Belgian-Dutch*

*coastal zone, southern bight of the North Sea*. Continental Shelf Research 23, 669-691

- [4] Gordon H.R., Wang M., 1994. *Retrieval of water-leaving reflectance and aerosol optical thickness over the oceans with SeaWiFS: a preliminary algorithm*. Applied Optics 33-3, 443-452
- [5] Park Y., De Cauwer V., Nechad B., Ruddick K., 2003. *Validation of MERIS water products for Belgian coastal waters: 2002-2003*. European Space Agency. WPP-223
- [6] Mueller J.L., Davis C., Arnone R., Frouin R., Carder K., Lee Z.P., Steward R.G., Hooker S., Mobley C.D., McLean S., 2000. *Above-water reflectance and remote sensing reflectance measurements and analysis protocols*. Ocean Optics protocols for satellite ocean color sensor validation Revision 2, p.98-107, National Aeronautical and Space Administration, Greenbelt, Maryland.
- [7] Nechad B., De Cauwer V., Park Y., Ruddick Y., 2003. *Suspended Particulate Matter (SPM) mapping from MERIS imagery. Calibration of a regional algorithm for the Belgian coastal waters*. European Space Agency. SP-549.
- [8] Gons H.J., 1999. *Optical teledetection of chlorophyll-a in turbid inland waters*. Environmental Science and Technology.33, 1127-1133.
- [9] Cutter M., Private Communication.